ARTICLE NO. 78-1197

Techniques for the Experimental Investigation of the Near Wake of a Circular Cylinder

R. W. Wlezien* and J. L. Way†
Illinois Institute of Technology, Chicago, Ill.

Several techniques used in an experimental investigation of the near wake of a circular cylinder in crossflow for Reynolds numbers from 5800 to 10,400 are discussed. A thermal tag is applied to one of the cylinder boundary layers prior to separation, and the instantaneous strength of the contaminant is detected downstream by an array of high resolution differential resistance thermometers. A generalized form of phase conditioning is used to determine phase-averaged properties of the amplitude and frequency modulated wake. Examples of results obtained using the present techniques are given, including typical phase-conditioned mean and rms wake temperature profiles, and statistics of the amplitude and frequency modulated phase reference signal.

Nomenclature

A = instantaneous amplitude of a modulated signal
D = diameter of the circular cylinder
f = frequency
f_s = sampling frequency of digitized data
Hi = Hilbert transform
i = imaginary unit
L_d = diffusion length scale
L_f = formation length scale
r = real bandlimited function
$\hat{r}$ = Hilbert transform of r
R = Fourier transform of r
$\hat{R}$ = Fourier transform of $\hat{r}$
Re = Reynolds number based on cylinder diameter
t = time
u = velocity component in X direction
U = phasing velocity $= \sqrt{u^2 + v^2}$
U_L = phasing velocity with periodic content suppressed
U_R = periodic component of phasing velocity
U_∞ = freestream velocity
v = velocity component in Y direction
X = streamwise coordinate nondimensionalized with cylinder radius
Y = cross-stream coordinate nondimensionalized with cylinder radius
z = complex analytic signal
θ = deviation from freestream temperature
ξ = Hilbert transform dummy variable
ϕ = instantaneous phase of a modulated signal

Introduction

A PICTURE of shear flow turbulence is emerging which is characterized by an assembly of repetitive, though not strictly periodic, structures that interact strongly as they move with the flow, with the large-scale structures remaining coherent over large downstream distances. The wake of a bluff body is a flowfield in which the formation and evolution of these structures can be observed readily. In order to lay the groundwork for measurements relating to wake evolution, techniques have been developed for the study of wake formation. The underlying mechanisms of the near wake have proved to be particularly elusive, and the methods presented here rely on the nearly periodic nature of the flow around a cylinder to develop a spatial picture of the wake. These techniques utilize an extension of periodic conditional sampling to processes that are not strictly periodic, but which, like the near wake, are modulated in both amplitude and phase.

Based on experiments and qualitative observations, the vortex shedding phenomenon has been classified into several distinct regimes summarized by Morkovin.[1] The regime of particular interest here is termed "subcritical," and is characterized by transition to turbulence after boundary-layer separation, with the transition point approaching the cylinder with increasing Reynolds number. Although this regime extends from $Re \approx 300$ to $Re \approx 1.3 \times 10^5$, the techniques discussed here have only been applied in the range $5800 < Re < 11{,}600$.

An interesting aspect of this regime is the relative insensitivity of Strouhal number to Reynolds number. Gerrard[2] has postulated that this is a consequence of opposing mechanisms in the near wake. The downstream distance at which the Karman vortex forms decreases with increasing Reynolds number, and this tends to increase the eddy shedding frequency. But the shear layers become unstable sooner after separation, so the vorticity is more diffuse at the point of eddy formation and the shedding frequency tends to be reduced. These offsetting mechanisms could account for the constant Strouhal number. Gerrard has proposed two wake length scales, the formation length L_f and the diffusion length L_d, which are characteristic of these mechanisms.

L_f is a measure of the downstream distance at which the Karman vortices are formed. Bloor,[3] Bloor and Gerrard,[4] and Schaefer and Eskinazi[5] have used various single-point measurement techniques to infer this length scale, but its definition remains somewhat arbitrary. Even more vague is the concept of L_d, a scale indicative of the diffusion of the separated shear layer with increasing downstream distance. Gerrard[6] used a two-sensor technique to estimate the instantaneous shear layer thickness, but more objective methods for scaling the near wake remain to be developed.

Another characteristic that further complicates a mechanistic understanding of the near wake for subcritical Reynolds numbers is the low-frequency wake modulation, an order of magnitude lower in frequency than the eddy shedding

Received June 29, 1978; presented as Paper 78-1197 at the AIAA 11th Fluid and Plasma Dynamics Conference, Seattle, Wash., July 10-12, 1978; revision received Feb. 5, 1979.

Index categories: Jets, Wakes, and Viscid-Inviscid Flow Interactions; Nonsteady Aerodynamics; Research Facilities and Instrumentation.

*Research Assistant. Mechanics and Mechanical and Aerospace Engineering Dept.

†Associate Professor. Mechanics and Mechanical and Aerospace Engineering Dept. Member AIAA.

(see Bloor[3] and Maekawa and Mizuno[7]). Rather than being strictly periodic with a well-defined shedding frequency, the wake is a modulated, polychromatic flowfield, characterized by spectra having peaks of finite bandwidth.

Phase conditioning has been used to advantage in the study of strictly periodic flowfields found in rotating machinery. Phase-conditioned averaging permits the conversion of single-point temporal data taken at many spatial positions during the independent experimental runs into average spatial data at a particular phase of the periodic flow. Near-wake temporal measurements, such as those by Maekawa and Mizuno[7] and Toebes,[8] while yielding valuable insight into wake mechanisms, are also open to subjective interpretation. DeCoster and Kibens,[9] Cantwell,[10] and Davies[11] have demonstrated the power of phase conditioning in wake flow. The technique presented here is a generalization of phase conditioning that is applicable to processes that are modulated both in amplitude and frequency.

Analysis

Phase-conditioned averaging techniques have been used by several workers in the study of wake flow. DeCoster and Kibens[9] treated the velocity fluctuations in the wake of a disk as the sum of mean, strictly periodic, and random components. Peak values in a velocity signal in the wake were used as a phase reference, and the periodic component of the wake velocity was then determined by ensemble averaging across many periods of the shedding cycle, using the reference signal peaks to initiate each realization at the ensemble. Davies[11] employed a similar technique in the wake of a D-shaped cylinder. Maxima in the signal obtained from a hot wire that senses fluctuations induced in the potential flow outside the wake were taken as the phase reference, and were used to trigger an ensemble average of velocity time series two Strouhal periods in length. Cantwell[10] utilized a modified technique in the wake of a circular cylinder. The modulated signal obtained from a surface pressure port was filtered and then tracked by a phase locked loop. The time interval between the initiation of two successive cycles was subdivided into 16 equal phase increments and all velocity samples occurring within a particular phase window were averaged.

Each of these techniques has its particular advantages and limitations. The methods of DeCoster and Kibens, as well as Davies, require only the determination of maxima in the reference signal to trigger the averaging. It is then a straightforward process to ensemble average the time series in the proximity of the phase reference. However, as Davies[11] says, "... the pattern at the edges of the cycle will become smeared if the period is too variable." In other words, if there is significant frequency modulation, the triggered ensemble averaging of time series will not be equivalent to true phase averaging. DeCoster and Kibens limit the periodic averaging to times when the phase reference signal passes a certain periodicity criterion, but it is not clear that this criterion will eliminate the smearing due to frequency modulation.

It is possible that the sharp separation lines of the disk and D-shaped cylinder limit the frequency modulation in these wakes. Mattingly,[12] in dye visualization studies in the wake of a circular cylinder, concludes that the axial irregularity in a wake vortex line produces a similar irregularity in the separation line, and this irregularity is then propagated to subsequent vortices. This modulation mechanism would be inhibited for bodies having fixed separation lines; therefore, the averaging techniques used by DeCoster and Kibens,[9] and Davies[11] might well be adequate.

The wake of a circular cylinder is amplitude and frequency modulated (see Fig. 5), hence greater care must be used in obtaining a phase-conditioned average. Cantwell's[10] technique takes the cycle-to-cycle variability of the period into account by linearly interpolating the phase between the end points of each cycle. The use of a phase-locked loop makes the hardware a little more complicated, but the phase computation is a straightforward linear interpolation. Its use is limited to signals having a frequency modulation, such that the frequency does not change very fast within a cycle, but instead changes slowly from cycle to cycle.

The technique used here is a generalization of the phase conditioning concept which is useful even when the modulation is large (or fast). It involves the application of a Hilbert transform (realized here as a digital filter) to a band-limited signal and the construction of a complex rotating vector from which phase, frequency, and amplitude can be directly computed at each sample time. These time series, which correspond to sampled continuous functions, can be treated as any other time series. For example, the instantaneous amplitude can be used to further condition the wake statistics, and the phase, frequency, and amplitude time series themselves can be analyzed statistically.

Figure 1 is the normalized power spectral density for the phasing signal U obtained in the potential flow near the separation line of the cylinder boundary layer. Although there is a distinct peak in the spectrum, this peak has a finite bandwidth characteristic of modulated signals. The velocity fluctuations contributing to the energy in this peak are a result of the flow induced by the Karman vortices, and are therefore indicative of the phase of the shedding process.

The first task in processing this phasing signal is to band-limit the signal to remove the undesired fluctuations outside the band of interest. Although it is possible to apply an analog bandpass filter to the signal before processing, nonrecursive finite impulse response (FIR) digital filters offer distinct advantages for this application. Since a phase angle is the quantity to be computed, any device (such as an analog filter) that introduces phase shifts into the data is undesirable. It can be argued from a causality standpoint that a real-time analog filter without phase shifts is impossible to construct. This causality problem does not apply to recorded digital signals because it is possible to look forward as well as backward in time. By using a nonrecursive digital filter which has an impulse response symmetric about zero time, no phase shifts are introduced into the data (see Ref. 13). This is equivalent to knowing the magnitude of a signal before it actually occurs in a real-time situation.

Mathematical techniques have been developed for constructing the instantaneous phase and amplitude of a band-limited function. It has its basis in the definition of an envelope given by Rice[14] for a function consisting of a finite sum of cosines, each having a distinct magnitude and phase. Rice's formula is very cumbersome, and its analytical use and explicit calculation is very difficult, except for simple signals. Dugundji[15] demonstrated that an envelope of a modulated signal equal to that given by Rice can be calculated by using a

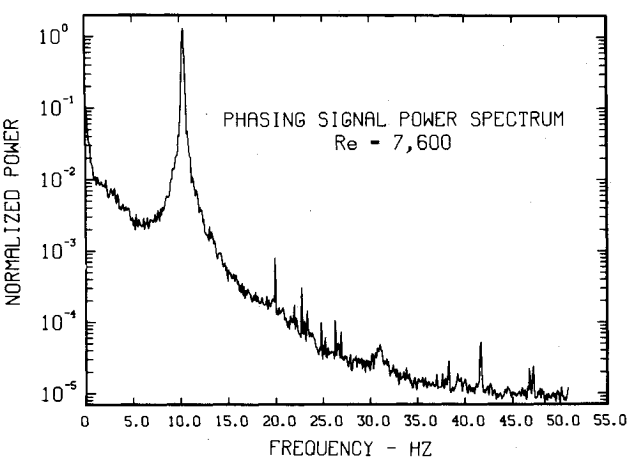

Fig. 1 Power spectrum of phasing signal.

Hilbert transform to construct a pre-envelope or analytic signal. The concept of an analytic signal was first introduced by Gabor,[16] and it permits a straightforward calculation of the instantaneous phase and amplitude for a given band-limited signal. Born and Wolf[17] have used this representation of real polychromatic fields in the theory of partially coherent light.

Given a real function $r(t)$, the Hilbert transform is defined by the infinite convolution:

$$\hat{r}(t) = Hi[r(t)] = \frac{1}{\pi}\int_{-\infty}^{\infty} \frac{r(\xi)}{\xi - t}\,d\xi \tag{1}$$

If $R(f)$ is the Fourier transform of $r(t)$, then $\hat{R}(f)$, the Fourier transform of $\hat{r}(t)$, is:

$$\hat{R}(f) = \begin{cases} +i\,R(f) & f>0 \\ 0 & f=0 \\ -i\,R(f) & f<0 \end{cases} \tag{2}$$

Hence, the Hilbert transform is an all-pass filter which changes the phase of each spectral component by $+\pi/2$ for positive frequencies by $-\pi/2$ for negative frequencies.

If a complex function $z(t)$ is constructed, such that,

$$z(t) = r(t) - i\hat{r}(t) \tag{3}$$

where $z(t)$ is called an analytic signal, or the pre-envelope of $r(t)$, then $r(t)$ can be said to be the real part of the complex rotating vector $z(t)$ (see Fig. 2). The functions $\hat{r}(t)$ and $z(t)$ are uniquely specified by $r(t)$, and if $z(t)$ is expressed in the polar form

$$z(t) = A(t)e^{i\phi(t)} \tag{4}$$

then $A(t)$ is the instantaneous envelope of $z(t)$ and $r(t)$, while $\phi(t)$ is the instantaneous phase.

A property of the function $z(t)$ is that its Fourier transform $Z(f)$ vanishes for all negative frequencies. In fact, $z(t)$ can be constructed by computing $R(f)$, setting $R(f)$ equal to zero for negative frequencies, and then inverse transforming to get $z(t)$. In practice, however, this can only be done for time-limited functions (like the turbulent spots of Gaster[18]) because the Hilbert transform is an infinite convolution. In this work, a finite impulse response approximation of the Hilbert transform is used to overcome this limitation.

Experiment

In order to follow the mechanics of the near wake, the vortical fluid in the separated region behind the cylinder must be detected. Due to the wide range of velocity magnitude and direction in the near wake, conventional hot-wire velocity measurements are extremely difficult, although novel approaches such as the flying hot wire of Cantwell[10] have been successful. Based on previous experience with thermal tracers,[19] the tracer technique was chosen as most viable for the present work. A slight amount of heat is transferred into one of the cylinder boundary layers before separation; for a fluid having a Prandtl number near one, the thermal boundary layer is of the same order of thickness as the momentum boundary layer. All the vortical fluid in one of the separated shear layers is tagged at its source, and this easily identifiable scalar indicates the downstream motion of the vorticity.

The cylinder model is a 5-cm-diam pyrex glass tube with a 25-deg arc of its surface coated with a thin gold film for use as a resistance heater (Fig. 3). The film is produced by firing a metallorganic compound to a cylinder surface at high temperatures. Because the film is only about 1000 Å thick, it produces no disturbance in the cylinder boundary layer. Early experiments indicated that the cylinder heating is not localized to the strip. Under steady-state conditions, the entire cylinder attained a temperature slightly above ambient and vorticity in both cylinder boundary layers received the thermal tracer. A two-dimensional, finite-difference model showed that coolant water circulated through the cylinder model and maintained at the same temperature as the ambient air would localize the cylinder heating to the near vicinity of the gold strip. A recirculating water system was constructed, and through the duration of the experiment, the water temperature was never allowed to deviate more than 0.04° C from the ambient wind-tunnel temperature. For a 60-cm-long heating strip, the typical power input was 60 W, resulting in a maximum air temperature of 2° C above ambient.

Measurements were conducted in the 90×60 cm high-speed test section of the I.I.T. Environmental Wind Tunnel. Since the 60-cm-long cylinder has a length-to-diameter ratio of 12, end plates were designed to effectively isolate the cylinder wake from the tunnel sidewall boundary layers. Flow visualization studies were conducted using smoke in the I.I.T. Flow Visualization Wind Tunnel, and the results indicate two primary considerations in end plate design. Upstream of the cylinder, the plates should be blunt enough to prevent flow separation, but large enough to prevent the stagnation streamlines from curving toward the wind-tunnel walls. The upstream portion of the plate should extend no more than about $D/4$ ahead of the cylinder with a thickness of about $D/8$. Downstream of the cylinder, the plates should be large enough to prevent communication between the near wake and the side wall boundary layers. The end plates used in this work extended about $4D$ downstream of the cylinder.

The phasing velocity signal was obtained by placing a hot-wire sensor parallel to the cylinder just outside the boundary layer near the separation line, as shown in Fig. 3. The magnitude of this signal was sufficiently small compared to

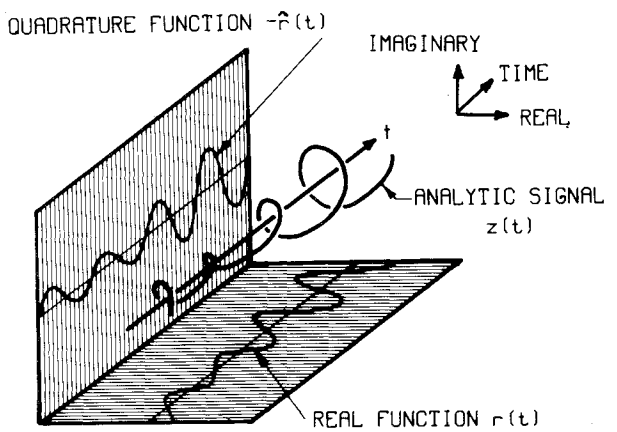

Fig. 2 Complex analytic representation of a real bandpassed signal.

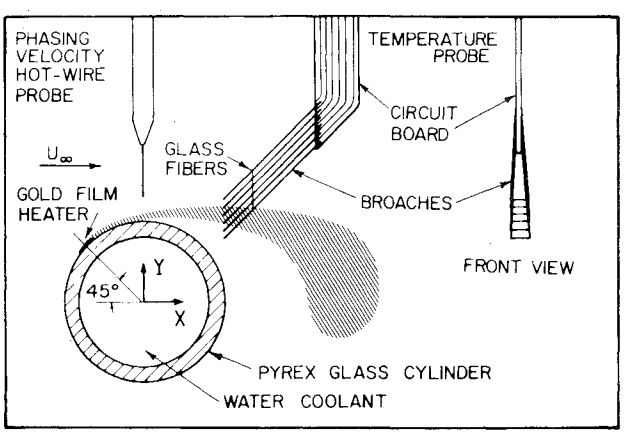

Fig. 3 Schematic of near-wake experiment.

the mean freestream velocity that no linearization was required. The signal was merely biased to a zero mean, amplified, and digitized.

The temperature measurements were bound by several constraints, including compensation for ambient temperature drift, high-frequency response, high resolution, and minimum flow interference. In order to reduce experiment run time to a reasonable duration, a 6-sensor probe was constructed to allow simultaneous temperature measurements at several spatial positions. Platinum-10% rhodium wires of 0.5 μm diameter were used as resistance thermometers, and they exhibited a frequency response of about 1-2 kHz. To compensate for wind-tunnel ambient temperature drift, the multichannel thermometer circuit described by Wlezien and Way[20] was constructed. This circuit uses a single ambient sensor to compensate all six wake sensors, and is exactly linear in wake-sensor resistance. With additional amplification, the thermometer circuitry provided a sensitivity of 4 V/°C with a noise level equivalent to 0.01°C rms.

The thermometer probe was of special low-interference design, since flow visualization diagnostics indicated that any body having a large stagnation area can drastically alter the near wake. A two-sided printed circuit board with conductors etched into its surface was mounted parallel to the mean flow, and jewelers broaches were soldered to pads on the board at a 45-deg angle to form the sensor supports. The sensors were mounted parallel to each other, 0.254 cm apart. Because of their extreme fragility, any vibration of the long broaches would result in sensor destruction, so a truss consisting of fine glass fibers was constructed about 1 cm from the sensors to tie the broaches together. This was sufficient to protect the wires from breakage during the course of all the experiments.

Data Acquisition and Processing

The I.I.T. data acquisition and processing system was used to sample and digitize analog data and to perform a portion of the data processing. The system is built around a PDP-11/10 processor, with a 16-channel, 12-bit analog-to-digital converter used for signal acquisition. Data are acquired directly into memory using a programmable clock to set the sampling rate, and the digital data are then stored on magnetic tape for further processing. Other peripherals include a graphic display and hard copy unit, a hardware multiply/divide unit, and a 60-cycle line frequency clock. A more detailed description of the system is given by Way.[21] The majority of the data processing was accomplished on the I.I.T. Univac 1108 computer, a large time-shared system.

In a typical data acquisition configuration, data are sampled and stored in memory until an entire block is completed, then the sampling is stopped and the data are recorded on tape. When digital filtering is required, it becomes desirable to acquire long blocks of continuous data. Due to hardware limitations, particularly in computer memory size, it is not desirable to have physical magnetic tape record lengths of more than a few thousand samples. Therefore, it becomes necessary to write the data on tape in multiple blocks with the data continuous between blocks. The flexibility of the computer-based acquisition system permits continuous acquisition using a double buffering technique. Data recorded at each spatial position consists of essentially one continuous time series of 153,000 samples.

Data were acquired at three Reynolds numbers using the continuous acquisition program. Due to the change in shedding frequency with Reynolds number, the sampling rates were adjusted so that the number of samples per shedding period was maintained at approximately 74. This essentially nondimensionalized the data with respect to sampling frequency so that identical filters could be applied to the data for all three runs. Temperature data were acquired at 80 probe positions in the wake, resulting in 480 individual temperature time series, each containing 200 Strouhal cylces of data. In addition to the six temperature channels, the phasing velocity was also simultaneously acquired and recorded digitally on magnetic tape.

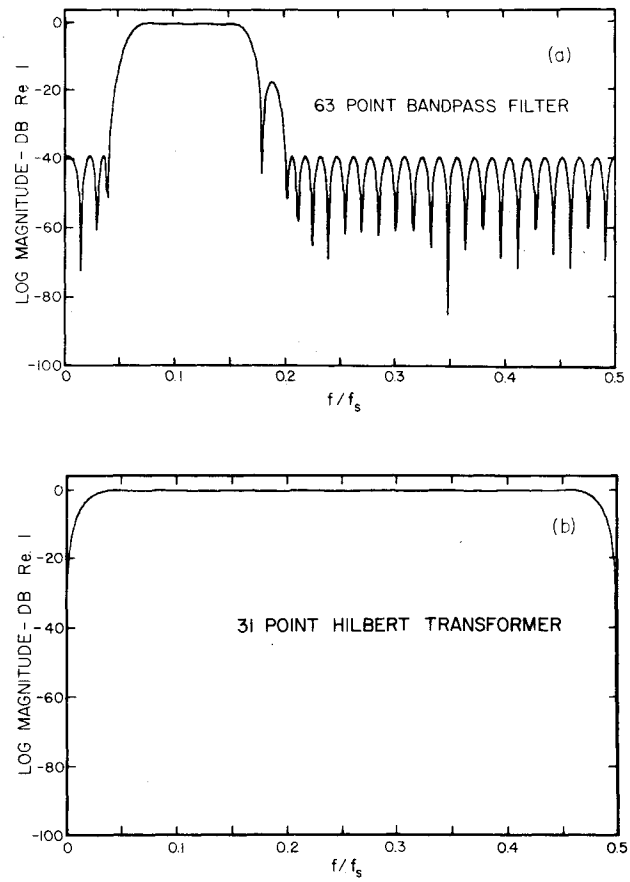

Fig. 4 Frequency response plots of FIR: a) bandpass filter; b) Hilbert transformer.

The discrete implementation of a bandpass filter and Hilbert transformer requires a certain amount of care. Given a filter response in the frequency domain, the time domain representation will, in general, be infinite in duration. An approach known as finite impulse response filtering involves the approximation of an infinite impulse response by a finite sequence. A naive way to determine this finite sequence is to simply truncate the infinite sequence. This can lead to large errors in frequency response due to Gibbs phenomenon. An optimization program written by McClellan and listed in Rabiner and Gold[13] has been used to generate the optimal equiripple filters used in the present work.

Since the sampling rate corresponds to 74 samples/Strouhal cycle, the phasing signal is grossly oversampled. The energy in the sampled signal is concentrated in an extremely small band relative to the Nyquist frequency; hence, the required digital filter would need to have sharp changes in amplitude response over a very small frequency band. This can only be accomplished by using a very long and computationally inefficient digital filter.

In order to produce a more reasonably sampled signal, the sampling rate must be effectively reduced through data decimation before an efficient filter can be constructed. Decimation by eight, that is, using only every eighth value of the phasing signal time series in computations, yields a more reasonably sampled signal. However, this decimation cannot, in general, be carried out blindly. Only if the signal has negligible spectral content at frequencies above the decimated Nyquist frequency will be the decimated signal be free from aliasing.

The frequency response of the filter used to process the phasing signal is shown in Fig. 4a. This filter has a 63-point

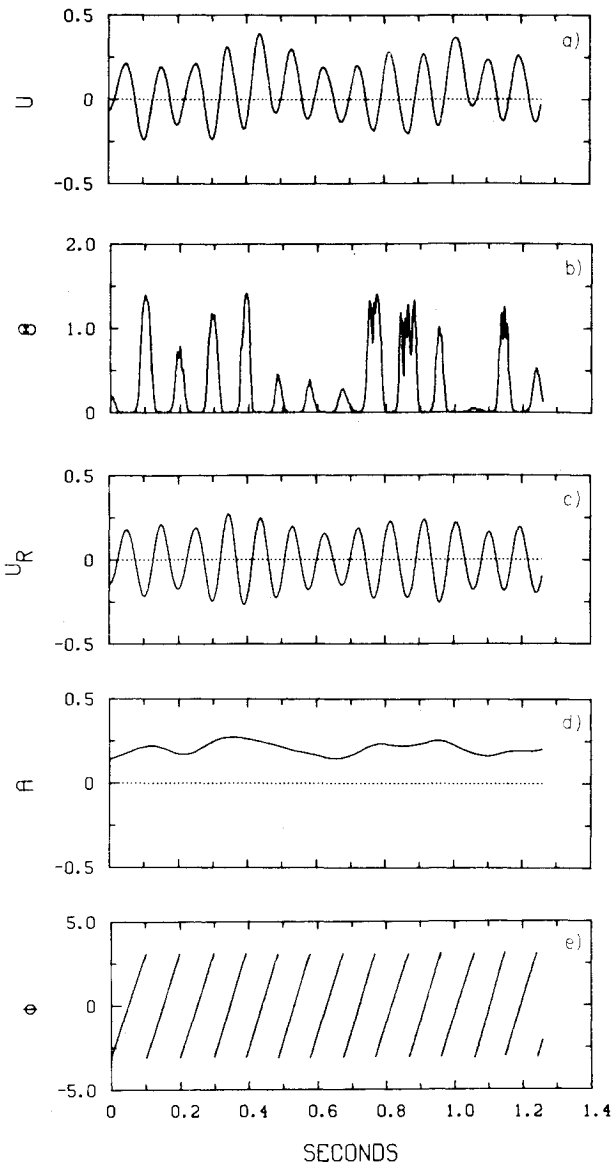

Fig. 5 Typical raw and computed time series.

impulse response, and bandpass filtering is accomplished by digitally convolving the filter with the decimated phasing signal time series. This particular filter was chosen after a parametric run of the design program; a general conclusion is that low error can only be achieved at the cost of filter length and selectivity.

The Hilbert transformer is implemented as a relatively short digital filter. The primary problem in designing a Hilbert transformer is the step discontinuity in the frequency response about zero frequency. The 31-point Hilbert transformer used to process the present data was also designed using the McClellan program, and its frequency response is shown in Fig. 4b.

Care must be also be taken when convolving the filter weights with the sampled data, as a portion of the time series required to start the filters is lost in the filtering process. For the 63-point filter and the 31-point Hilbert transformer, a total of 46 data values are lost. The continuous acquisition process permits the filtering to be continued across record gaps, resulting in a significant reduction in lost data.

In order to be able to conditionally sample all the acquired temperature data, the sampling rate of the computed phase and amplitude functions must be restored to that of the original phasing signal. This requires an interpolation routine

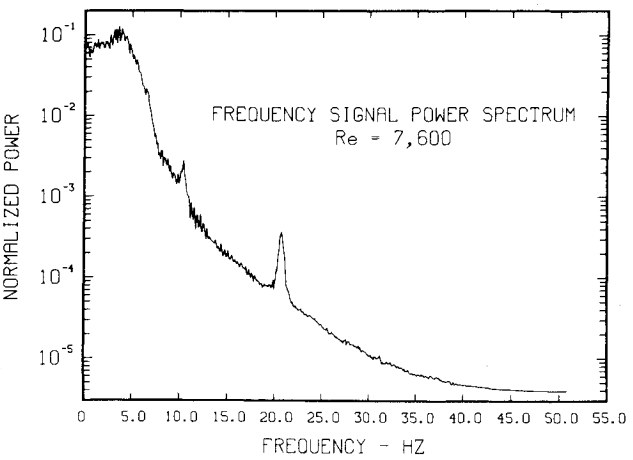

Fig. 6 Power spectrum of frequency computed from phasing signal.

to increase the sampling rate by a factor of eight. Since the results of the phase and amplitude computations are functions which are not aliased, the interpolation process can also be accomplished through filtering (see Crochiere and Rabiner[22]). The missing data are simply filled with zeros and, after low-pass filtering, the sampling rate is increased without altering the shape of the signal spectrum.

Results

Examples of results obtained for $Re = 7600$ will be discussed here to demonstrate the scope of the present techniques. Figure 5a is a sample of the phasing velocity signal which has the power spectrum of Fig. 1. Two features should be noted: there is modulated periodicity in a band near 10 Hz and there are less regular fluctuations at lower frequencies. The content near 10 Hz can be immediately identified with the Strouhal frequency of the wake, and a similar periodicity is exhibited in the simultaneous wake temperature signal of Fig. 5b. The fluctuations in the temperature signal appear to be phase related to the periodic part of the phasing signal, although there is variation in the temperature signal from cycle to cycle.

The digital bandpass filter is applied to the phasing signal to extract the periodic content, and this yields the signal U_R shown in Fig. 5c. The low-frequency fluctuations are no longer present and U_R is in phase with the periodic variations in U. The analytic signal is then constructed, with U_R taken as the real part and $\hat{U}_R$, its Hilbert transform, taken as the negative imaginary part. Amplitude and phase can be determined from this pre-envelope through Eq. (4).

Figure 5d is the instantaneous amplitude computed for this segment of U_R. It varies slowly in comparison with the shedding frequency and a simple visual evaluation of several records indicates a somewhat ramp-like structure, slowly growing and decaying. The amplitude modulation is rather large in magnitude, with a root mean square value equal to 30% of the mean.

The phase function of Fig. 5e is computed as the instantaneous angle that the complex vector $z(t)$ makes with the positive real axis (see Fig. 2). It is a continuous function of time, except when a branch cut is made to keep the phase on a single branch of the complex plane. Although ϕ appears to have a constant slope or frequency, further analysis of the data verifies the presence of frequency modulation. The frequency time series is formed by numerically differentiating the phase time series. For these data, the rms frequency modulation is 4% of the mean, or about 0.4 Hz, with the peak deviations, of course, being considerably greater.

The time series computed through this decomposition can be treated as any other time series in order that statistics such as correlations and spectra can be computed. For example, Fig. 6 is the power spectrum of the frequency time series.

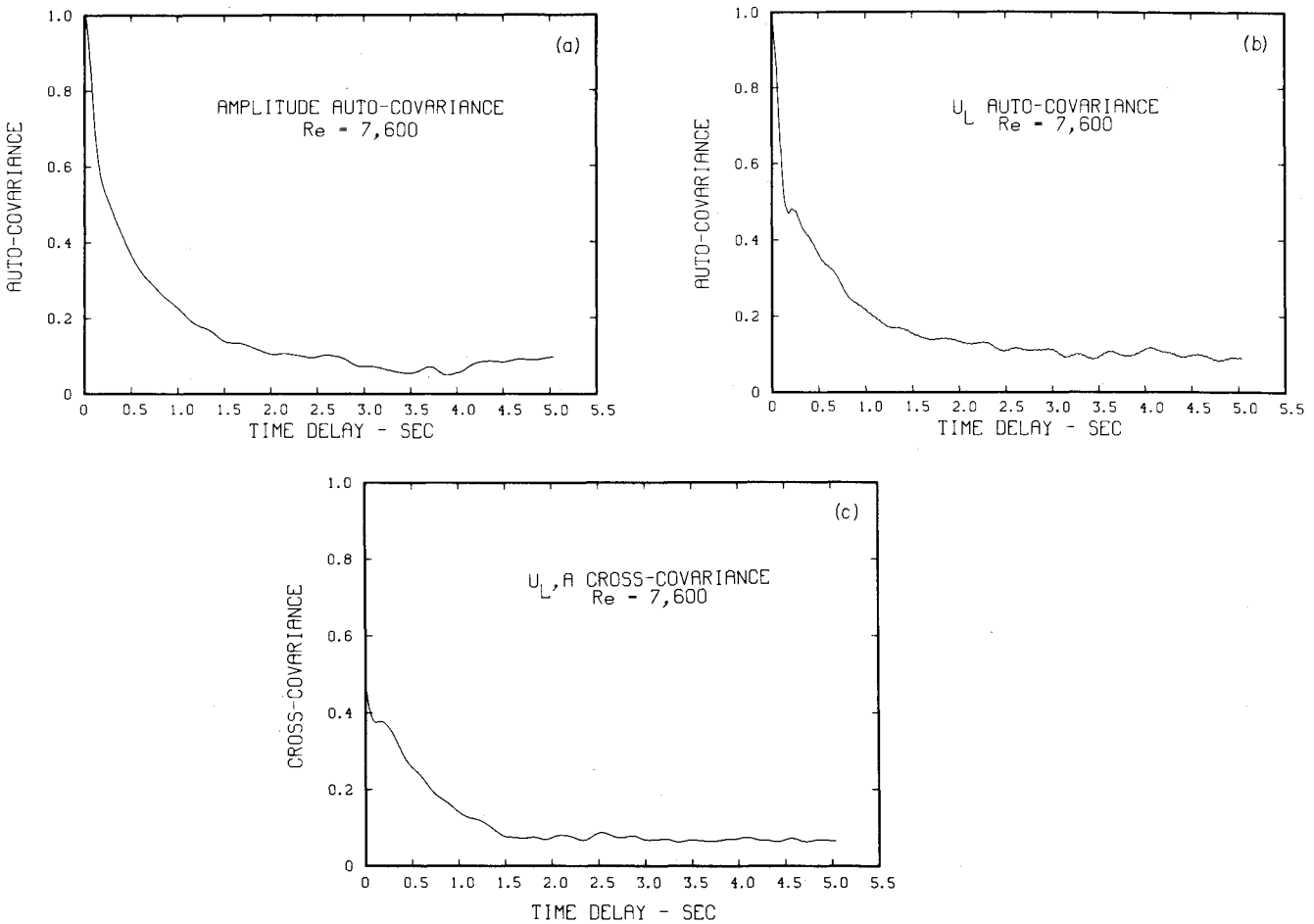

Fig. 7 Covariance functions for the computed amplitude and the phasing signal with periodicity suppressed.

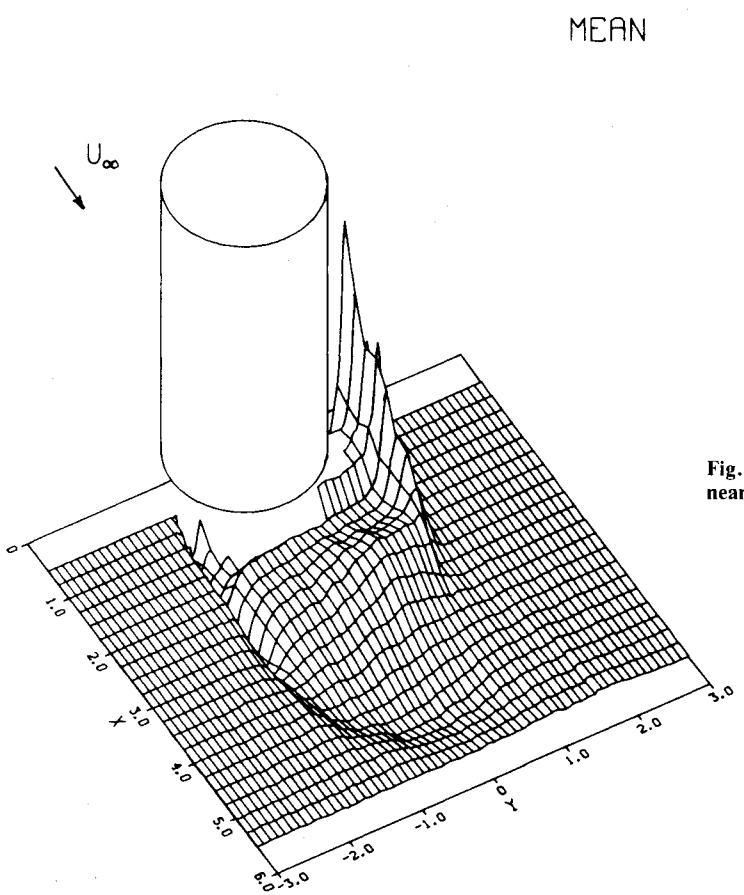

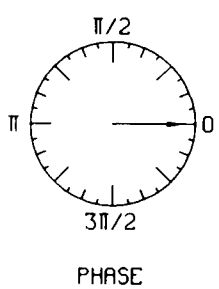

Fig. 8 Typical phase-conditioned mean temperature distribution in near wake.

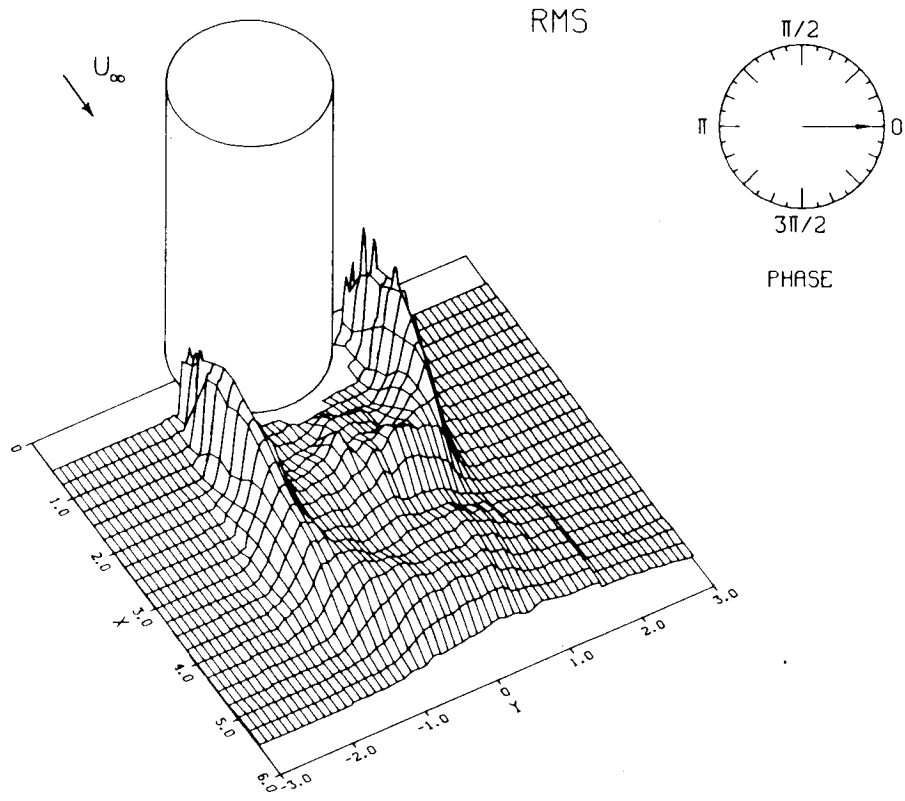

Fig. 9 Typical phase-conditioned root mean square temperature distribution in near wake.

Although it might be unusual to discuss the frequency distribution of frequency fluctuations, this statistic is simply an indication of how fast the Strouhal frequency is being modulated. The sharp peaks near 10 and 20 Hz are a consequence of the discrete Hilbert transformer. These peaks can be made arbitrarily small by increasing the duration of the Hilbert transformer. The broad peak around 4 Hz is of particular interest because it yields some insight into the frequency deviations in the wake. This peak corresponds to approximately 40% of the Strouhal frequency. Thus, when an eddy shedding cycle proceeds rapidly, the shedding frequency will tend to drop below the mean within one to two cycles. The frequency regulating mechanism in the near wake appears to act over spans of a few cycles rather than over spans of many cycles.

Figure 7a is a plot of autocovariance of the amplitude time series. The correlation initially drops very fast, with a decrease of 40% within two shedding cycles. The correlation appears to be significant for time delays much larger than the Strouhal period, and, in fact, the record length for the present data seems to be insufficient for the autocovariance to decay to zero. Visual examination of the data indicates that the amplitude fluctuations appear to be related to the low-frequency content in the phasing signal. A new function U_L was formed, which corresponds to the phasing signal U with the contribution near the eddy shedding frequency suppressed, i.e.,

$$U_L = U - U_R \tag{5}$$

Figure 7b is the autocovariance of U_L, and it is remarkably similar to the autocovariance of A. The cross-covariance between A and U_L, shown in Fig. 7c, demonstrates that A and U_L are indeed highly correlated, with a maximum correlation coefficient of 0.48. The relationship between these two signals, however, is not fully understood at this time.

The phase function of Fig. 5e was used to conditionally sample the wake temperature data. The shedding cycle was subdivided into 32 discrete phases, and all temperature data for a particular wake position and phase were averaged. Further conditioning can be performed using the amplitude and frequency functions, although no such results are presented here.

Figures 8 and 9 present the phase-conditioned mean and rms temperature as the vertical coordinate of a surface above the x-y plane behind the cylinder. Both plots are for a phase of zero, and the cylinder height corresponds to 2°C for the mean temperature and 1°C for the rms surface. The rms temperature is an indication of the magnitude of temperature fluctuations about the value on the mean temperature plot for the same phase. A total of 32 such surfaces have been plotted for the mean and rms temperatures, and a movie has been made which sequences through these plots for a series of cycles. The temperature values for the lower shear layer corresponding to negative Y were constructed symmetrically across the wake centerline using values at a phase removed by π rad from the given phase. The signs for the mean values in the two shear layers were chosen to simulate the sense of vorticity that is indicated by the temperature. The jaggedness noticeable in the shear layers close to the cylinder is a manifestation of the surface plotting routine, the data being rather smooth there.

The mean surface shows the thin separated shear layer spreading and decreasing in magnitude in the downstream direction, eventually rolling up into the Karman vortex, which is seen as a small hill in the surface. The depression near the wake centerline farther downstream is the previous vortex shed from the lower side of the cylinder. The movie clearly shows each vortex being formed at a fixed location and its subsequent acceleration from rest and convection downstream. Also evident in the movie is the transverse motion of the shear layer at the Strouhal frequency.

The rms temperature in both shear layers is seen to increase to a maximum before decreasing. The increase corresponds to growth of the Bloor instabilities in the early laminar portion of the layer. The movie shows that, in general, the rms is higher at the edge of the Karman vortex than it is at the vortex center, although this is not evident from Fig. 9 alone. Similar results have been computed for other Reynolds numbers so that systematic comparisons can be made.

Conclusions

We have demonstrated that the thermal tracer technique is a viable method for studying the near wake of a bluff body. A slight amount of heat transferred into one of the boundary layers tags the vortical fluid, making it detectable in the wake. A velocity signal from a single hot-wire sensor, placed in the potential flow near the separation line, has been decomposed using a discrete implementation of the Hilbert transform. This decomposition yields an instantaneous phase time series even when large amplitude and frequency modulation are present. Conditional temperature distributions were obtained by conditioning the near wake temperature averages on the phase time series. These wake profiles show the formation and shedding of an average vortex, and should yield intracycle information on the scaling of the near wake. Furthermore, the Hilbert transform method produces amplitude and frequency time series which are available for further processing. Intercycle statistics have been obtained for the near wake data from these time series.

Acknowledgment

The authors would like to express their appreciation to M. V. Morkovin and H. M. Nagib for their advice and assistance. We also thank an anonymous reviewer for his helpful criticism. We are grateful to V. Mattioli for her typing effort. Research was sponsored by the Air Force Office of Scientific Research (AFSC), U.S. Air Force, under Contract F44620-76-C-0062.

References

[1] Morkovin, M. V., "Flow Around a Circular Cylinder—A Kaleidoscope of Challenging Fluid Phenomena," *Symposium on Fully Separated Flows*, ASME, 1964.

[2] Gerrard, J. H., "The Mechanics of the Formation Region of Vortices Behind Bluff Bodies," *Journal of Fluid Mechanics*, Vol. 25, Pt. 2, 1969, p. 401.

[3] Bloor, M. S., "The Transition to Turbulence in the Wake of a Circular Cylinder," *Journal of Fluid Mechanics*, Vol. 19, Pt. 2, June 1964, p. 290.

[4] Bloor, M. S. and Gerrard, J. H., "Measurements on Turbulent Vortices in a Cylinder Wake," *Proceedings of the Royal Society of London A*, Vol. 294, 1966, p. 319.

[5] Schaefer, J. W. and Eskinazi, S., "An Analysis of the Vortex Street Generated in a Viscous Fluid," *Journal of Fluid Mechanics*, Vol. 6, 1959, p. 241.

[6] Gerrard, J. H., "Experimental Investigation of a Separated Boundary Layer Undergoing Transition to Turbulence," *The Physics of Fluids Supplement*, 1967, p. S98.

[7] Maekawa, T. and Mizuno, S., "Flow Around the Separation Point in the Near-Wake of a Circular Cylinder," *The Physics of Fluids Supplement*, 1967, p. S184.

[8] Toebes, "The Unsteady Flow and Wake Near an Oscillating Cylinder," *Journal of Basic Engineering*, Paper 68-WA/FE-23, 1968.

[9] DeCoster, M. A. and Kibens, V., "Periodic Vortex Shedding in a Wake of a Disk," Tech. Rept., University of Michigan, May 1974.

[10] Cantwell, B. J., "A Flying Hot-Wire Study of the Turbulent Near Wake of a Circular Cylinder at a Reynolds Number of 140,000," PhD. Thesis, California Institute of Technology, 1976.

[11] Davies, M. E., "A Comparison of the Wake Structure of a Stationary and Oscillating Bluff Body, Using a Conditional Averaging Technique," *Journal of Fluid Mechanics*, Vol. 75, May 1976, Pt. 2, pp. 209-231.

[12] Mattingly, G., "An Experimental Study of the Three Dimensionality of the Flow Around a Circular Cylinder," Tech. Note BN-295, University of Maryland, 1962.

[13] Rabiner, L. and Gold, B., *Theory and Application of Digital Signal Processing*, Prentice Hall, Englewood Cliffs, New Jersey, 1975.

[14] Rice, S. O., "Mathematical Analysis of Random Noise," *Bell System Technical Journal*, Vols. 23 and 24, 1944, pp. 1-162.

[15] Dugundji, J., "Envelopes and Pre-Envelopes of Real Waveforms," *Institute of Radio Engineers Transactions on Information Theory*, Vol. IT-4, March 1958, pp. 53-57.

[16] Gabor, D., "Theory of Communications," *Journal of IEE*, Vol. 93, 1946, Pt. III, pp. 93-429.

[17] Born, M. and Wolf, E., *Principle of Optics*, Pergamon Press, Oxford, 1965.

[18] Gaster, M., "A Theoretical Model of a Wave Packet in the Boundary Layer on a Flat Plate," *Proceedings of the Royal Society of London A.*, Vol. 347, 1975, pp. 271-289.

[19] Fabris, G., "Conditionally Sampled Turbulent Thermal Velocity Fields in the Wake of a Warm Cylinder and its Interaction with an Equal Wake," Ph.D. Thesis, Illinois Institute of Technology, May 1974.

[20] Wlezien, R. W. and Way, J. L., "Bridge Circuits for Differential Resistance Thermometry," *International Congress on Instrumentation in Aerospace Simulation Facilities*, IEEE, Sept. 1977, pp. 89-94.

[21] Way, J. L., "Applications in Fluid Mechanics Research of a Portable Data Acquisition and Processing System," *International Congress on Instrumentation in Aerospace Simulation Facilities*, IEEE, Sept. 1975, pp. 50-58.

[22] Crochiere, R. E. and Rabiner, L. R., "Optimum FIR Digital Filter Implementations for Decimation, Interpolation, and Narrow-Band Filtering," *IEEE Transactions on Acoustics, Speech and Signal Procedures*, Vol. ASSP-23, No. 5, Oct. 1975, pp. 444-456.